Self-Driven Phase Transitions Drive Myxococcus xanthus Fruiting Body Formation

Guannan Liu, Adam Patch, Fatmagül Bahar, David Yllanes, Roy D. Welch, M. Cristina Marchetti, Shashi Thutupalli, and Joshua W. Shaevitz

Phys. Rev. Lett. **122**, 248102 — Published 20 June 2019

DOI: 10.1103/PhysRevLett.122.248102

A self-driven phase transition drives *Myxococcus xanthus* fruiting body formation

Guannan Liu,[1,*] Adam Patch,[2,*] Fatmagül Bahar,[3,*] David Yllanes,[2,4,*] Roy D. Welch,[3] M. Cristina Marchetti,[2] Shashi Thutupalli,[1,†] and Joshua W. Shaevitz[1,‡]

[1] *Joseph Henry Laboratories of Physics and Lewis-Sigler Institute for Integrative Genomics, Princeton University, Princeton, NJ 08544, USA*

[2] *Department of Physics and Soft and Living Matter Program, Syracuse University, Syracuse, NY 13244, USA*

[3] *Department of Biology, Syracuse University, Syracuse, NY 13244, USA*

[4] *Instituto de Biocomputación y Física de Sistemas Complejos (BIFI), 50009 Zaragoza, Spain*

(Dated: May 1, 2019)

Combining high-resolution single cell tracking experiments with numerical simulations, we show that starvation-induced fruiting body (FB) formation in *Myxococcus xanthus* is a phase separation driven by cells that tune their motility over time. The phase separation can be understood in terms of cell density and a dimensionless Péclet number that captures cell motility through speed and reversal frequency. Our work suggests that *M. xanthus* take advantage of a self-driven non-equilibrium phase transition that can be controlled at the single cell level.

Unicellular organisms such as bacteria and amoeba are capable of spontaneously organizing into complex multicellular structures [1, 2]. A striking example of such collective behavior is the starvation-induced organization of the rod-shaped, soil-dwelling bacterium *Myxococcus xanthus* into macroscopic, multicellular aggregates known as "fruiting bodies" (FBs) [3]. When nutrients are scarce, *M. xanthus* cells undergo a multicellular process of self-organization during which cells move to form dome-shaped aggregates comprising hundreds of thousands of cells. A subset of cells at the center of each droplet differentiate to form metabolically quiescent spores that can survive long periods of starvation [3–5].

The striking phenotypic similarity between FB formation in *M. xanthus* and in the amoeba *Dictyostelium discoidium* has led to the longstanding hypothesis that *M. xanthus* FB formation is driven by long-range chemical signaling mechanisms, as it is in the amoeba. Although *M. xanthus* cells are thought to employ chemical communication to initiate FB formation (termed A-signaling) [6], to synchronize reversal frequency (termed C-signaling) [7, 8], and to communicate through mucopolysaccharide "slime trails" that other cells can sense and follow [9], a quantitative understanding of the mechanisms that drive aggregation has remained elusive.

M. xanthus cells move by gliding on solid surfaces using both tank-tread-like transport motors and the retraction of extruded filaments called pili, and can modulate their speed in a continuous manner [10, 11]. The cells also have the ability to reverse their direction of motion, typically every several minutes, and can modify the reversal frequency in different situations [12–14]. In addition to the role of chemical signaling, previous modeling work has attempted to investigate mechanical aspects of FB formation by considering contact-mediated interactions between cells, although these ideas have not been thoroughly tested experimentally [15].

Using experiments and insight from theory, we demonstrate that *M. xanthus* FB formation can be described as a phase separation process driven, at least initially, by changes to the motility of individual cells. Importantly, this appears to happen in the absence of complex signaling mechanisms and interactions between cells, and requires no real-time control at the cellular level. While the ability to actively change motility ultimately leads to a phase transition, cells do not have to implement a complicated feedback mechanism to alter motility in response to specific chemical or mechanical cues. Rather, cells need only speed up and suppress reversals upon starvation and the collective mechanics then naturally induces phase separation of the entire population. The theoretical inspiration for this work is the Motility-Induced Phase Separation (MIPS), where purely repulsive Active Brownian Particles (ABPs) spontaneously aggregate through a jamming-based phase transition [16–18]. While there are important differences between the MIPS and the droplet formation seen in *M. xanthus* populations, we use this model to explore parameters and regions of phase space that are inaccessible to experiments.

We first investigated the dynamics of FB formation using different cell densities (experimental details are described in the Supplemental Materials, SM). Time-lapse, bright-field images were used to quantify the resultant dynamics (Fig. 1, Movies S1-3). Pixel intensity is indicative of local population density with darker regions corresponding to the FBs and the lighter pixels corresponding to the low density regions of bacteria. When the inoculation cell density is very low (2.5×10^7 cells/mL), no large-scale structure formation is seen (Movie S1). Over the first few hours, cells largely move independently, reversing frequently and with minimal cell-cell contacts and interactions. This results in the formation of spatially stable nematic streams at later times ($\sim$ 6-8 hours) but not fruiting bodies [14].

* These authors contributed equally to this work.

† Present address: Simons Center for the Study of Living Machines, National Centre for Biological Sciences, Tata Institute for Fundamental Research, Bangalore 560065, India

‡ E-mail: shaevitz@princeton.edu

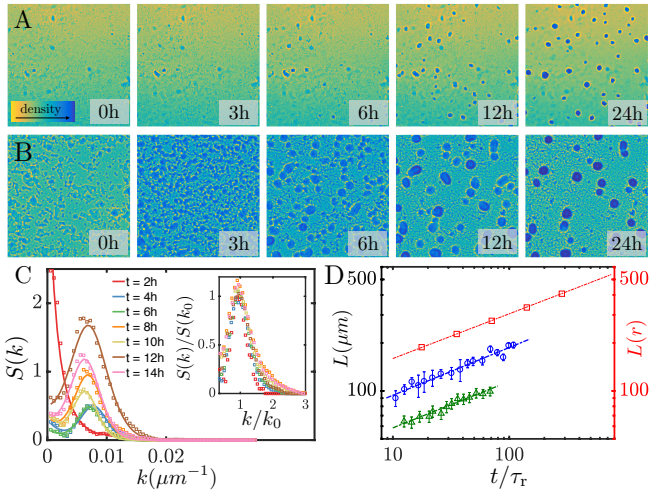

FIG. 1. Aggregation in *M. xanthus*. (A, B) Microscopy images of *M. xanthus* cells undergoing phase separation via a nucleation and growth process (A, low density at 1.5×10^8 cell/mL) and spinodal decomposition (B, high density at 5×10^8 cell/mL). Each image has dimension 1.5 mm by 1.5 mm. (C) The structure factor at different spatial frequencies for *M. xanthus* phase separation at high density and different times after starvation is calculated as the magnitude squared of the radial component of the Fourier transform of images. Solid lines are fits to the sum of a Gaussian function and a decaying exponential. Time $t = 0$ denotes the first frame in a movie where macroscopic coarsening is observed. (C, inset) Collapse of the radial Fourier transform when frequency is scaled by the peak wavenumber k_0 and the amplitude is scaled by the peak amplitude $S(k_0)$. (D) Power law scaling of the dominant length scale with time, $L \sim t^\alpha$, for nucleation and growth (green triangles, $\alpha = 0.29 \pm 0.02$) and spinodal decomposition (blue circles, $\alpha = 0.30 \pm 0.02$) experiments (left axis), and ABP spinodal decomposition simulations (red squares, $\alpha = 0.281 \pm 0.002$, right axis). Time is written in units of the reversal time, $\tau_r \approx 10$ min. Error bars represent one standard-error.

When the inoculation density is increased to 1.5×10^8 cells/ml, FBs form randomly in space and time through the experiment (Fig. 1A, Movie S2). In a field of view of 3 mm by 2.5 mm, approximately 10 FB droplets were observed after 24 hours, although in some cases as few as 2 droplets formed. This spatio-temporally random appearance of FBs is similar to a phase separation process called nucleation and growth in which an energy barrier between two phases causes small fluctuations in the population density to die out. The later stages of coarsening involve significant flux between neighboring FBs, seen directly in some experiments where the cell movement is evident and in others where small droplets are observed to dissolve into nearby larger ones. This is reminiscent of an Ostwald ripening process and recent work used a model of Ostwald ripening to predict the disappearance and persistence of *M. xanthus* FBs [19].

When the inoculation density was further increased to 5×10^8 cells/mL and above, we observed that FBs formed via a different dynamical mechanism (Fig. 1B, Movie S3). Rather than spatially random nucleation and slow growth, high-density cultures spontaneously and immediately begin to phase separate over the entire field of view. Within the first 11 hours after plating (Fig. S1), we observed the formation of a global instability in the cell density that resulted in small, mesh-like structures that cover the petri dish. This kind of spontaneous phase separation, similar to spinodal decomposition, classically arises when microscopic fluctuations in the local density are inherently unstable, lacking an energy barrier to separate the homogeneous and more favorable phase-separated regimes. As the mesh coarsened over time, small droplets appeared that were connected by thinner layers of cells. Finally, a subset of these droplets grew and turned into round FBs. We determine if an experiment exhibits phase separation and the underlying kinetic mechanism by analyzing the temporal dynamics in the image as described in the SM.

We next compared the dynamics of FB formation to the well-studied MIPS seen in simulations of ABPs. Briefly, we simulated particles moving with speed v_0 along a direction that is randomized at rate D_r and reversed at rate $f_{\rm rev}$ (see SM for further details). As has been shown previously, and similar to our observations from *M. xanthus* cells, ABPs aggregate in a density-dependent manner [16–18]. At very low densities, no aggregation is observed (Movie S4), whereas the simulations produce nucleation and growth and finally spinodal decomposition as the density of particles is increased (Movies S5 and S6). In this model, aggregation occurs as particle-particle collisions cause jamming that can only be relieved though rotation of the orientation vectors.

A hallmark of spinodal decomposition is a well-defined length scale of the phase-separated domains that increases with time as a power-law as the domains grow self-similarly [20, 21]. At high inoculation densities corresponding to the spinodal regime, a single dominant length scale emerges in the organization of the bacterial domains (Fig. 1C) and grows in time as a power law with an exponent $\alpha = 0.30 \pm 0.02$ (Fig. 1D). When the structure factor $S(k)$ is rescaled by the peak wavenumber and amplitude, the shape of the peak remains largely constant over time up to 14 hours, representing self-similar coarsening of the phase separated domains (Fig. 1C inset) [20, 22] [23] . At later times, the initially mesh-like domains break up into rounder droplets in what appears to be a separate part of the phase separation mechanism. A similar increase in the dominant length scale with time is seen at low inoculation densities where the size of the individual aggregates in the nucleation and growth regime grows in time with the same exponent, $\alpha = 0.29 \pm 0.02$. We next measured the length scale for ABPs undergoing a MIPS and recover a similar scaling, $\alpha = 0.281 \pm 0.002$ [24] . These results are in agreement with previous results for non-reversing ABPs [25–27] and continuum models of MIPS [28]. Interestingly, we find that the time evolution of the characteristic size is the

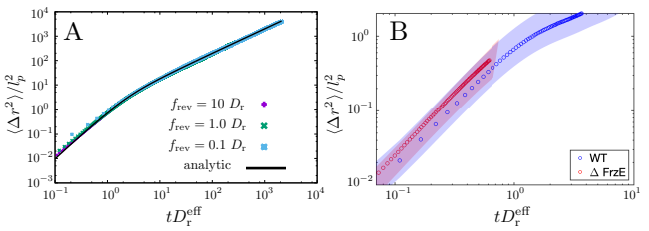

FIG. 2. Reversals affect rotational diffusion. (A) Mean square displacement (MSD) versus time for single particles, plotted for various reversal frequencies. The data for different reversal frequencies collapse when time is scaled by the reorientation time $\tau_r^{-1} = D_r^{eff}$. The solid line is described by Eq. S7. (B) Experimental MSD for isolated wild-type (blue) and ΔFrzE (red) *M. xanthus* cells. Time is scaled by $D_r^{eff,WT} = 0.336$ min^{-1} and $D_r^{eff,\Delta FrzE} = 0.065$ min^{-1}, respectively. Shaded regions represent the combined standard error taking into account uncertainty in the measured speed, reversal frequency, and D_r.

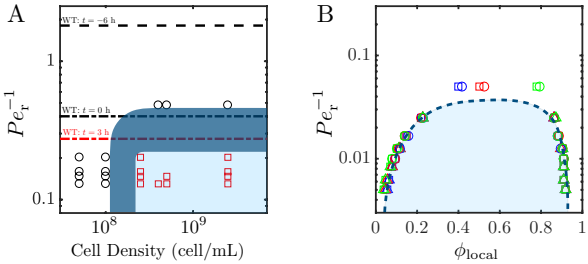

FIG. 3. (A) Experimental phase diagram for *M. xanthus* phase separation of the non-reversing mutant ΔFrzE. For each experiment at a particular density and Pe_r^{-1}, we determined whether the system is phase separated via spinodal decomposition (red squares) or not phase separated (black circles) after 24 hours. The estimated region of phase space containing the spinodal line is shaded in dark blue while the spinodal region is shaded in light blue. Dashed horizontal lines denote the Pe_r^{-1} for wild-type cells one hour after inoculation (t=−6 h), at the moment coarsening is first observed (t=0 h), and 3 hours into the coarsening process (t=3 h). (B) The phase diagram for reversing ABPs showing the spinodal boundary. Spinodal points correspond to the peaks of a bimodal distribution of local density (see SM) for different values of the ratio $f_{rev}/D_r = 0.1$(triangles), 1(squares), 10(circles) and of the packing fraction $\phi_0 = 0.45$(blue), 0.55(red), 0.65(green). The dashed line is a guide to the eye. The horizontal axis is the local particle packing fraction ϕ_{local}.

same for active 2D aggregation (MIPS simulation) and *M. xanthus* FB formation.

We next sought to investigate the effect of changes in motility on FB formation. The total activity in self-propelled systems can be quantified using the dimensionless inverse rotational Péclet number, given by the ratio of the cell size ℓ_c to the persistence length of the motility paths $\ell_p = v_0/D_r$ [25–27, 29],

$$\mathrm{Pe}_r^{-1} = \ell_c/\ell_p = \ell_c D_r/v_0\ . \tag{1}$$

As *M. xanthus* cells can spontaneously reverse their direction of motion at rate f_{rev}, we sought to understand how these reversal events might change the Péclet number. Introducing a reversal frequency adds a new timescale, the effects of which can be incorporated in an effective rotational diffusion coefficient (see SM and [30])

$$D_r^{eff} = D_r + 2f_{rev}\ . \tag{2}$$

We confirmed that Equation 2 accurately describes the trajectories from both simulations and moving cells. Adding reversals as a Poisson process with mean frequency f_{rev} to a model of ABPs [16, 18, 31], we found that the single-particle mean squared displacement (MSD) for different reversal frequencies collapses when time is scaled by the reorientation time $\tau_r^{-1} = D_r^{eff}$ (Fig. 2A). Moreover, the crossover between ballistic and diffusive motion occurs at time $t = \tau_r^{-1}$ for all f_{rev} at both low and high particle density (Fig. S6).

To measure the effect of reversals on trajectories of moving cells, we performed experiments at very low cell density so that the motion of individual cells was not affected by cell-cell collisions and motion was purely two-dimensional, as opposed to the three-dimensional motion in the FBs (Fig. S2A). The velocity autocorrelation function for the WT cells calculated from these data decays exponentially with small scale oscillations that die out at longer times due to the directional reversals (Fig. S2B). We fit the autocorrelation functions from both the wild-type (WT) and the non-reversing mutant ΔFrzE [32] and found that $D_r^{eff,\ WT} = 0.336$ min^{-1} and $D_r^{eff,\ FrzE} = 0.065$ min^{-1}. When time is scaled by these values of D_r^{eff}, the MSD versus time plots for WT and ΔFrzE cells collapse together. Interestingly, with a measured wild-type reversal frequency of 6.3 h^{-1}, this implies that the underlying rotational diffusion coefficient of WT cells, $D_{r,WT} = 0.127$ min^{-1} is larger than that of ΔFrzE cells, $D_{r,FrzE} = 0.065$ min^{-1}, potentially indicating the the Frz pathway may affect directionality in addition to reversal.

If FB formation is an actively driven process, changes to Pe_r^{-1} could affect the occurrence of cellular aggregation as it does in the MIPS. To control the Pe_r^{-1} of *M. xanthus* experimentally, we used non-reversing ΔFrzE cells and altered the propulsion speed v_0 using the drug nigericin [33]. The inverse Péclet number for each experimental condition was estimated by separately measuring cell velocity and D_r, combined with the average cell size of $\ell_c = 2.5$ μm (half a cell length). We mixed a small number of fluorescently-labeled cells with non-fluorescent cells at a ratio of 1:400 and tracked the fluorescent cells to measure their speed. We find that the velocity of ΔFrzE cells decreases monotonically from 1.25 μm/min in the absence of drug to 0.36 μm/min in the presence of 10 μM nigericin (Fig. S2C). By tracking isolated cells at very low density, we find that D_r does not change

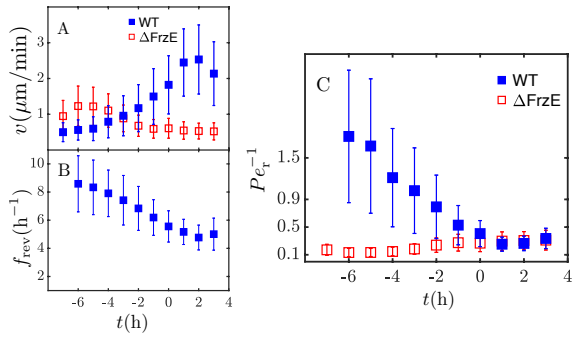

FIG. 4. Cell tracking over time after starvation. Cell speed (A), reversal frequency (B), and the resulting $\mathrm{Pe}_\mathrm{r}^{-1}$ (C) are shown for wild-type (blue) and non-reversing ΔFrzE cells (red). ΔFrzE cells do not reverse, so no red points are plotted in B. Error bars represent the standard error of the mean. $t = 0$ corresponds to 7 hours post inoculation, when macroscopic coarsening was first observed in these experiments.

when nigericin is added up to a concentration of 10 μM (Fig. S2D), in contrast to the effect in eukaryotes [34].

We generated a phase diagram for *M xanthus* FB formation by performing experiments with ΔFrzE cells at different inoculation densities and nigericin concentrations (Fig. 3A). When starved, non-reversing cells coarsen into FBs with the same temporal scaling as WT cells, although these aggregates are unstable and short lived (Fig. S7, Movies S7 and S8). As predicted, at low density or high $\mathrm{Pe}_\mathrm{r}^{-1}$, the system does not form FBs (black circles). At high density or low $\mathrm{Pe}_\mathrm{r}^{-1}$, the system phase separates via spinodal decomposition (red squares). The estimated region of the phase space that includes the spinodal line is shaded in dark blue on the phase diagram, and at high density lies between $\mathrm{Pe}_\mathrm{r}^{-1} = 0.20$ and 0.48. In Fig. 3B, we show a similar phase diagram obtained from simulations of reversing ABPs. The scaling of the data for different values of f_rev and mean density confirms that the effect of reversals can be incorporated into $\mathrm{Pe}_\mathrm{r}^{-1}$ using the effective rotational diffusion coefficient $D_\mathrm{r}^\mathrm{eff}$. Our results are in good agreement with previous studies of ABPs without reversals [26, 27].

$\mathrm{Pe}_\mathrm{r}^{-1}$ depends on four parameters, two of which *M. xanthus* potentially has the ability to control during FB formation. Cells do not grow during aggregation due to the starvation conditions and D_r is presumably set by thermal fluctuations of the cell body and molecular noise in the motility process. However, both the cell speed v_0 and the reversal frequency f_rev are known to be under cellular control, suggesting that the cells might have adapted to take advantage of such control [33, 35].

We tracked individual fluorescent wild-type cells at a population density of 5×10^8 cell/mL for 11 hours after starvation and found cells changed both their gliding speed and reversal frequency (Fig. 4). In the first 2–3 hours, cells exhibited low gliding speeds of $\sim 1.3\mu$m/min. By the time macroscopic coarsening was first observed, about 7 hours after starvation ($t = 0$), *M. xanthus* cells had sped up to $\sim 2.5\mu$m/min (Fig. 4A). We observed that wild-type cells became more active over the time course of our experiment (Fig. S3), in agreement with previous reports of an initial "resting" phase upon starvation [36] [37] . We also found that reversal frequency decreased from 8.5 h^{-1} to 5 h^{-1} over the coarse of the experiment, with most of the reduction occurring before $t = 0$ (Fig. 4B).

A combination of increased v_0 and decreased f_rev produces a reduction in $\mathrm{Pe}_\mathrm{r}^{-1}$ from $\sim$ 1.8 before starvation to $\sim$ 0.25 when mature fruiting bodies have been formed (Fig. 4C). Most of this reduction occurs in the first 7 hours after starvation, and $\mathrm{Pe}_\mathrm{r}^{-1}$ plateaus at the same time as the onset of macroscopic coarsening ($t = 0$, Fig. 3). The apparent critical $\mathrm{Pe}_\mathrm{r}^{-1} \sim 0.3$ lies in the region of phase space that we estimate to include the spinodal line. We note that the phase diagram in Figure 3 is made by examining the behavior of non-reversing cells that do not alter their behavior over time (Fig. 4A). The correspondence between the critical $\mathrm{Pe}_\mathrm{r}^{-1}$ at which starving wild-type cells start to undergo macroscopic coarsening and the estimated spinodal line derived from ΔFrzE cells strongly indicates that $\mathrm{Pe}_\mathrm{r}^{-1}$ is sufficient for understanding the initial process of phase separation.

To further test this idea, we added nigericin to starving WT cells and found that above a concentration of 2.5μM, the population was unable to form FBs. This is likely due to the inability of these cells to speed up enough to cross the critical $\mathrm{Pe}_\mathrm{r}^{-1}$. Finally, it is possible that *M. xanthus* cells could alter their reversal frequency directly as a function of cell density, explaining the observed reduction in f_rev over time. However, we measured reversal frequency for isolated cells and did not observe any significant change in reversal frequency (Fig. S4).

Here we present a simple physical picture of *M. xanthus* FB formation based on the statistical physics of active populations. Before starvation, cells move slowly and reverse frequently, favoring a homogeneous population on the surface. Upon starvation, wild-type cells speed up and reverse less often, producing a situation favorable for phase separation and FB formation. However, fruiting body formation is ultimately a sophisticated biological process and it is likely that our simple model does not capture the entirety of its complexity. Many of the details that we purposely left out of our analysis could play a role in the specific evolution and shape of the final fruiting bodies. These include cell-cell alignment, the effects of "slime following," and cell-cell communication via the C- and A-signaling mechanisms. For example, ΔFrzE cells do not form stable fruiting bodies. While initially stable, droplets typically fall apart at the end of 24 hours, towards the end of traditional FB development. This potentially indicates that additional biological or chemical mechanisms could play a role in FB stability over long times. More complicated models of *M. xanthus* aggregation may uncover the role of these additional parameters [see e.g. ref 38], but it is unlikely that they will

change the basic features we have observed here.

The two-dimensional ABP model we used differs from FB formation in several important ways. ABPs phase separate via a jamming aggregation process where the particles slow down due to crowding, whereas *M. xanthus* cells remain motile throughout the process of FB formation (see e.g. Movie S3 and S6). Importantly, the fruiting bodies are three-dimensional structures that appear to be 'dewetted' from the initial homogenously spread quasi-two-dimensional layer of cells. However, the similarity in the scaling exponents for coarsening and the phase diagrams may potentially indicate that these processes, while seemingly very different on the microscopic scale, may in fact belong to the same universality class of active systems. Future work tracking cells and monitoring droplet shape in three dimensions should lead to a more accurate theory of the phase separation which might be viewed as the dewetting of an active bacterial fluid layer into 3D droplets.

The authors thank Suraj Shankar and Lisa Manning for useful discussions and Suraj Shankar for the calculation of the MSD for ABPs with reversals. MCM was supported by NSF-DMR-1609208 and Simons Foundation Targeted Grant in the Mathematical Modeling of Living Systems 342354. MCM and AP acknowledge support by the NSF IGERT program through award NSF-DGE-1068780. MCM, AP and DY were additionally supported by the Soft Matter Program at Syracuse University. Simulations were carried out on the Syracuse University HTC Campus Grid supported by NSF-ACI-1341006. DY acknowledges partial support by from MINECO (Spain) and FEDER (European Union) FIS2015-65078-C2-1-P. JWS, ST, and GL were supported by NSF-PHY-1401506, NSF-PHY-1521553, the Center for the Physics of Biological Function NSF-PHY-1734030, and an HFSP Cross Disciplinary Fellowship to ST. RDW and FB were supported by NSF-DBI-1244295. Part of this work was performed at the Aspen Center for Physics, which is supported by NSF-PHY-1607611.

[1] M. T. Laub and W. F. Loomis, Mol Biol Cell **9**, 3521 (1998).
[2] D. Dormann, B. Vasiev, and C. Weijer, J Biol Phys **28**, 765 (2002).
[3] D. R. Zusman, A. E. Scott, Z. Yang, and J. R. Kirby, Nat Rev Microbiol **5**, 862 (2007).
[4] J. Starruß, F. Peruani, V. Jakovljevic, L. Søgaard-Andersen, A. Deutsch, and M. Bär, Interface Focus **2**, 774 (2012).
[5] L. J. Shimkets, Microbiol Rev **54**, 473 (1990).
[6] A. Kuspa, L. Plamann, and D. Kaiser, J Bacteriol **174**, 3319 (1992).
[7] S. Lobedanz and L. Søgaard-Andersen, Genes Devel **17**, 2151 (2003).
[8] L. J. Shimkets and H. Rafiee, J Bacteriol **172**, 5299 (1990).
[9] R. P. Burchard, J Bacteriol **152**, 495 (1982).
[10] R. Balagam, D. B. Litwin, F. Czerwinski, M. Sun, H. B. Kaplan, J. W. Shaevitz, and O. A. Igoshin, PLOS Comput Biol **10**, 1 (2014).
[11] J. Hodgkin and D. Kaiser, Mol Gen Genet **171**, 177 (1979).
[12] Y. Wu, A. D. Kaiser, Y. Jiang, and M. S. Alber, Proc Natl Acad Sci USA **106**, 1222 (2009).
[13] B. D. Blackhart and D. R. Zusman, Proc Natl Acad Sci USA **82**, 8767 (1985).
[14] S. Thutupalli, M. Sun, F. Bunyak, K. Palaniappan, and J. W. Shaevitz, J Royal Soc Interface **12**, 20150049 (2015).
[15] O. Sozinova, Y. Jiang, D. Kaiser, and M. Alber, Proceedings of the National Academy of Sciences **102**, 11308 (2005).
[16] Y. Fily and M. C. Marchetti, Phys Rev Lett **108**, 235702 (2012).
[17] M. E. Cates and J. Tailleur, Annu Rev Condens Matter Phys **6**, 219 (2015).
[18] M. Marchetti, Y. Fily, S. Henkes, A. Patch, and D. Yllanes, Curr. Opin. Colloid Interface Sci. **21**, 34 (2016).
[19] F. Bahar, P. C. Pratt-Szeliga, S. Angus, J. Guo, and R. D. Welch, Sci Rep **4**, 6376 (2014).
[20] A. J. Bray, Advances in Physics **51**, 481 (2002).
[21] P. M. Chaikin and T. C. Lubensky, *Principles of condensed matter physics* (Cambridge university press, 2000).
[22] J. Marro, J. L. Lebowitz, and M. H. Kalos, Phys. Rev. Lett. **43**, 282 (1979).
[23] $S(k)$ is typically normalized by the square of the peak wavenumber for a 2D system, but nonlinearities in our imaging and lighting make this unfeasible.
[24] Both motility-induced and equilibrium phase separation show a crossover from a faster growth law at short times, corresponding to the initial nucleation of clusters, to the slower coarsening regime shown in Fig. 1D. This short-time regime is not, however, accessible to experiments. The full kinetics of MIPS has been studied in [27].
[25] J. Stenhammar, A. Tiribocchi, R. J. Allen, D. Marenduzzo, and M. E. Cates, Phys Rev Lett **111**, 145702 (2013).
[26] G. S. Redner, M. F. Hagan, and A. Baskaran, Phys Rev Lett **110**, 055701 (2013).
[27] A. Patch, D. Yllanes, and M. C. Marchetti, Phys Rev E **95**, 012601 (2017).
[28] R. Wittkowski, A. Tiribocchi, J. Stenhammar, R. J. Allen, D. Marenduzzo, and M. E. Cates, Nature communications **5**, 4351 (2014).
[29] J. Bialké, J. T. Siebert, H. Löwen, and T. Speck, Phys Rev Lett **115**, 098301 (2015).
[30] R. Grossman, F. Peruani, and M. Bär, Physical Review E **94**, 050602(R) (2018).
[31] J. Tailleur and M. E. Cates, Phys. Rev. Lett. **100**, 218103 (2008).
[32] While ΔFrzE cells have been reported to reverse at a very low frequency, we did not observe any reversals using this strain in our analysis.
[33] M. Sun, M. Wartel, E. Cascales, J. W. Shaevitz, and T. Mignot, Proc Natl Acad Sci USA **108**, 7559 (2011).

[34] P. Maiuri, J.-F. Rupprecht, S. Wieser, V. Ruprecht, O. Bénichou, N. Carpi, M. Coppey, S. De Beco, N. Gov, C.-P. Heisenberg, *et al.*, Cell **161**, 374 (2015).
[35] M. Guzzo, S. M. Murray, E. Martineau, S. Lhospice, G. Baronian, L. My, Y. Zhang, L. Espinosa, R. Vincentelli, B. P. Bratton, *et al.*, Nature microbiology **3**, 948 (2018).
[36] L. Jelsbak and L. Søgaard-Andersen, Proc Natl Acad Sci USA **99**, 2032 (2002).
[37] ΔFrzE cells do not change speed when starving, indicating a link between the Frz pathway and gliding speed.
[38] C. R. Cotter, H.-B. Schüttler, O. A. Igoshin, and L. J. Shimkets, Proc Natl Acad Sci USA **117**, E4592 (2017).